Sponsored By:
American Institute of Aeronautics and Astronautics (AIAA)
Society of Automotive Engineers (SAE)
American Society of Mechanical Engineers (ASME)

AIAA-80-1192
Modeling Pressure Oscillations in Ramjets

F. E. C. Culick, California Institute of Technology, Pasadena, Ca.; and T. Rogers, The Marquardt Co., Van Nuys, Ca.

AIAA/SAE/ASME 16th JOINT PROPULSION CONFERENCE

June 30-July 2, 1980/Hartford, Connecticut

MODELING PRESSURE OSCILLATIONS IN RAMJETS

F. E. C. Culick*
California Institute of Technology
Pasadena, California

and

T. Rogers**
The Marquardt Company
Van Nuys, California

Abstract

Pressure oscillations in ramjet engines are approximated as one-dimensional motions and treated within linear acoustics. The exhaust nozzle is represented by the admittance function for a short choked nozzle. New results have been obtained for the quasi-steady response of a normal shock wave in the diffuser. Acoustic fields in the inlet region and in the combustion chamber are matched to provide an analytical expression of the criterion for linear stability. Combustion processes are accommodated but not treated in detail. As examples, data are discussed for two liquid-fueled engines, one having axial dump and one having side dumps.

I. Introduction

The high density and rate of energy release in a combustion chamber favor excitation and maintenance of pressure oscillations. If compensating influences acting to attenuate the oscillations are weak, then unsteady motions in the flow field may interfere with proper operation of the system. Recent concern (refs. 1, 2) with pressure oscillations observed in ramjet engines prompted the work discussed in this paper.

Experience with other systems showing similar problems - called generically "combustion instabilities" - is the basis for the viewpoint and approach taken here. The oscillations are regarded in first approximation as small amplitude acoustic waves propagating in a steady non-uniform flow field. One may then construct a framework for examining the influences of various processes on the structure of the waves and on their linear stability.

Stability may be expressed in terms of the gains and losses of energy for the acoustic waves. An unstable wave appears, to an observer, as a self-excited oscillation growing exponentially in time without limit, if the net gain of energy exceeds the net loss. In actual systems the growth of unstable waves does not continue indefinitely, a consequence of nonlinear behavior which we will not examine here (ref. 3).

The source of energy for unstable waves is ultimately associated with combustion. Energy flows to and from the acoustic fields as a consequence of interactions between the unsteady fluctuations and steady processes of combustion and flow. Representing those interactions poses the greatest difficulties in treating problems of combustion instability. In this work we accommodate them in a general fashion, but we do not analyze them in detail.

An instability in a propulsion system may usually be characterized by a small number of frequencies. These inevitably are close to the frequencies of the natural acoustic modes for the internal cavity of the system. The mechanisms for energy exchange with the acoustic waves also cause the frequencies to differ from those computed according to classical acoustics without combustion and flow; the shifts are usually small and often unobservable. Most previous work on oscillations in ramjets has dealt with "screech", or instabilities having relatively high frequencies, usually several kilohertz or more. The waves excited were essentially transverse acoustic modes for a cylindrical chamber. Contemporary engines of the sort discussed here exhibit more troublesome lower frequency instabilities closely related to longitudinal modes. The primary cause for concern with these oscillations is their effect on the inlet shock system and therefore on the usable pressure recovery of the engine.

It appears that only in Russian work has attention been seriously paid to longitudinal oscillations. Published accounts (refs. 3 and 4) are based largely on calculations which are inadequate for the problems we treat here. The approach followed here is therefore considerably different.

Compared with rocket engines, ramjets have two characteristics which produce some distinctive differences in the pressure oscillations observed: combustion is confined to a chamber which is a substantial part but not the whole of the volume of the system; and an important boundary condition is presented by the shock system located at the forward end of the inlet duct. The Mach number of the average flow in the inlet can be quite high and should not be ignored, whereas the Mach number of the flow in the combustion chamber is generally small.

In Section II the acoustics problem is formulated. We use a one-dimensional approximation to represent the fields in both the inlet duct and the combustion chamber. Boundary

*Associate Fellow, AIAA. Professor of Applied Physics and Jet Propulsion.

**Member, AIAA Senior Development Engineer.

conditions are specified as admittance functions for a choked nozzle at the exhaust plane and for a single normal shock at the entrance plane. The solutions for the two chambers are matched at the entrance to the combustion chamber, the "dump plane".

We have the unusual opportunity to compare data for pressure oscillations observed in two engines, LFRED and LIFRAM, having very different geometrical configurations. The LFRED engine has an axial dump with a single inlet, and LIFRAM has two inlets with a side dump arrangement. The differences appear here mainly in the structure of the acoustic oscillations excited in the combustion chamber.

The boundary condition presented to the acoustic field by the inlet shock is more important and interesting than we anticipated. This problem is treated in Section III, giving the real and imaginary parts of the admittance function for quasi-steady behavior of a normal shockwave.

Fortunately, data have been obtained at several locations in the engines. The pressure records have been filtered and analyzed to give the distributions of both amplitude and relative phase in both engines. These are compared with the theoretical results in Section IV. This appears to be the first detailed treatment of the phase distribution in an engine of any sort. The results suggest that more attention should be paid to this characteristic. Differences in the phase distributions helped guide the modelling of the acoustic fields in the two engines treated here. More specifically, the relative phases measured in the inlet ducts constitute a significant check of the calculations of the admittance function for a normal shock wave.

The amalgamation of analysis and experiment provides the basis for drawing quite definite conclusions in respect to the observed behavior, and suggests some guidelines for design. These matters are discussed in Section V.

II. Formulation of the Acoustics Problem

Figure 1 is a sketch of the geometry, an idealized representation of several contemporary engines using dump combustors. Observation of the unsteady behavior suggest that the lower frequency oscillations do not involve significant transverse motions anywhere in the engine, even with side-dump inlets. Hence, the analysis here is based on a one-dimensional model for a device having a coaxial inlet. Within this framework, a case with side-dump inlets is treated simply by using the appropriate total cross-section areas. For example, S_0 in Figure 1, the area at the position of the inlet shock, is really the sum of the areas where the inlet shocks are located in the multiple inlets.

Two examples motivate the analysis. The LFRED and LIFRAM engines sketched below in Figures 11 and 12. The first has a coaxial dump configuration with high inlet Mach number and large blockage at the entrance to the combustor. In contrast, LIFRAM has two side-dump inlets with little blockage. Emphasis is placed on conditions at the entrance to the combustor because although LFRED exhibits a wave mode in

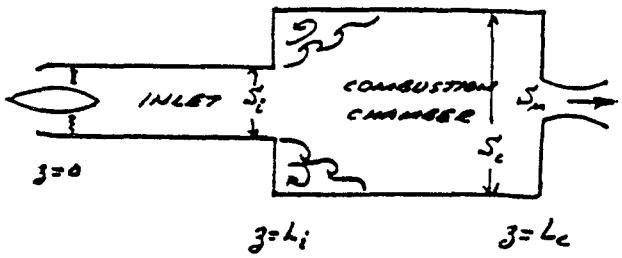

Fig. 1. Typical Geometry for a Ramjet Engine with a Dump Combustor.

the combustor, the pressure in LIFRAM has been observed to be nearly uniform in the combustion chamber, while oscillating under unsteady conditions. Part of the purpose here is to show how both sorts of behavior can be obtained from a single analysis.

Imagine that the engine is divided into two parts, the inlet and the combustion chamber, for each of which we postulate a representation of the acoustic field. The forms are chosen to satisfy the boundary conditions at the inlet diffuser and combustor.

2.1 Boundary Conditions and Admittance Functions

Boundary conditions will be specified as admittance functions. The definition of an admittance function is illustrated in Figure 2 and is given by the formula*

$$A = \frac{\vec{u}' \cdot \hat{n}/\bar{a}}{p'/\gamma \bar{p}} = \bar{\rho}\,\bar{a}\,\frac{\vec{u}' \cdot \hat{n}}{p'} \qquad (2.1)$$

where $\bar{a}_i = (\gamma \bar{p}_i/\bar{\rho}_i)^{\frac{1}{2}}$ average speed of sound in the inlet; mean values will always be denoted by $\bar{(\ )}$. It is important to note that the unit normal vector $\hat{n}$ always points outward from the column enclosed by the boundary. Thus, for example, in the case of oscillations only in the z-direction, when the region of interest lies in $0 \le z \le L$, then $\vec{u}' \cdot \hat{n} = -u'_z$ at $z = 0$, and $\vec{u}' \cdot \hat{n} + u'_z$ at $z = L$. From the definition of mass flux, $\vec{m} = \rho \vec{u}$, the fluctuations to first order are

$$\vec{m}' = \bar{\rho}\,\vec{u}' + \rho' \bar{\vec{u}} \qquad (2.2)$$

*Fluctuations denoted by $(\ )'$ contain the time dependence: $\varphi'(z,t) = \hat{\varphi}(z)\exp(-i\omega t)$.

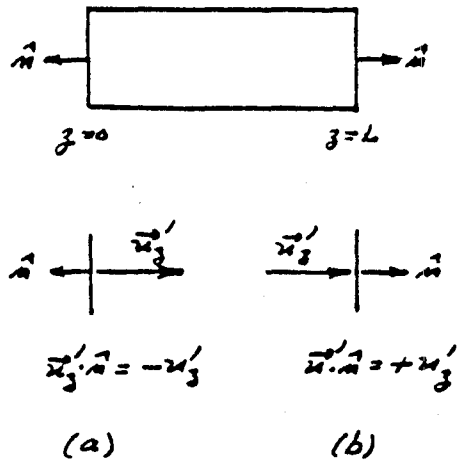

Fig. 2. Illustration for the Definition of Admittance Functions.

so if here we admit mean flow, (2.2) can be written

$$A = \bar{\rho}\,\bar{a}\left[\frac{\vec{m}'\cdot\hat{n}}{\bar{\rho}\,p'} - \frac{\rho'}{\bar{\rho}\,p'}\,\vec{\bar{u}}\cdot\hat{n}\right]$$

Let $\bar{m} = \bar{\rho}\vec{\bar{u}}\cdot\hat{n}$ be the average mass flux through the boundary, and the last relation is

$$A = \gamma\bar{M}\left[\frac{\vec{m}'\cdot\hat{n}/\bar{m}}{p'/\bar{p}} - \frac{\rho'/\bar{\rho}}{p'/\bar{p}}\right] \qquad (2.3)$$

where $\bar{M} = \bar{u}/\bar{a}$ is the Mach number of the mean flow. This definition will be used for the admittance function applied to the inlet and exit planes in Figure 1.

2.2 Acoustic Field in the Inlet

To simplify the analysis, we ignore variations of cross-sectional area. The rapid changes in the diffuser section will appear indirectly through their influence on the admittance function for the shock wave. Thus, we treat the problem of acoustic waves in a uniform flow field. If distributed losses in the inlet are ignored, a very good approximation, the governing acoustics equations are

$$\bar{\rho}_i\frac{\partial u'}{\partial t} + \bar{\rho}_i\bar{u}_i\frac{\partial u'}{\partial z} + \frac{\partial p'}{\partial z} = 0 \qquad (2.4)$$

$$\frac{\partial p'}{\partial t} + \bar{u}_i\frac{\partial p'}{\partial z} + \gamma\bar{p}_i\frac{\partial u'}{\partial z} = 0 \qquad (2.5)$$

where $(\,)_i$ denotes values in the inlet duct and u' stands for u'_z. The field consists of a wave travelling to the left and a wave travelling to the right; in steady state the superposition is a stationary wave pattern. Appropriate solutions to (2.4) and (2.5) are

$$p' = [P_+e^{ik_+z} + P_-e^{-ik_-z}]e^{-i\omega t}$$
$$u' = [U_+e^{ik_+z} + U_-e^{-ik_-z}]e^{-i\omega t} \qquad (2.6)a,b$$

in which the wave to the right (left) is denoted by + (-). Substitution of (2.6) a, b into (2.4) and (2.5) eventually leads to four linear equations relating the coefficients P_+, P_-, U_+, U_-. The condition for non-trivial solutions gives formulas for k_+ and k_-:

$$k_+ = \frac{k}{1+\bar{M}_i} \qquad k_- = \frac{k}{1-\bar{M}_i} \qquad (2.7)$$

The equations may then be used to relate the coefficients:

$$U_+ = \frac{1}{\bar{\rho}_i\bar{a}_i}P_+ \qquad U_- = -\frac{1}{\bar{\rho}_i\bar{a}_i}P_- \qquad (2.8)$$

so (2.6) a, b may be written

$$p' = [P_+e^{iKz} + P_-e^{-iKz}]e^{-i(\omega t+\bar{M}_iKz)}$$
$$u' = \frac{1}{\bar{\rho}_i\bar{a}_i}[P_+e^{iKz} - P_-e^{-iKz}]e^{-i(\omega t+\bar{M}_iKz)} \qquad (2.9)a,b$$

and

$$K = \frac{k}{1-\bar{M}_i^2} = \frac{(\omega - i\alpha)/\bar{a}_i}{1-\bar{M}_i^2} \qquad (2.10)$$

Note that the wavenumber is complex, the imaginary part, $\alpha/\bar{a}_i$, being nonzero because of losses in the system.

Treated in this way, the inlet appears as a classical impedance tube with mean-flow. The source of the leftward moving wave is the combustion chamber which we examine below. In steady state the leftward moving wave is reflected from the diffuser, generating the rightward moving wave. Both have constant amplitude, and so far as the stationary interference in the inlet is concerned, most details of the reflection process are unimportant. The influence of the diffuser is represented by an admittance function, A_o, which is set at the origin, $z = 0$. In Section III we discuss calculations of the admittance function for the simplest case of reflection by a single normal shock wave. For convenience we define the admittance function A_o to be the negative of the definition (2.1), and shown in Figure 2a:

$$A_o = \bar{\rho}_i\bar{a}_i\frac{u'}{p'} \qquad (2.11)$$

Substitution of (2.9) a, b into (2.11) leads to the relation between P_+ and P_-, $P_+ = \beta P_-$ with

$$\beta = \frac{1+A_o}{1-A_o} \qquad (2.12)$$

Because this is a linear problem, the amplitude of the oscillations cannot be unambiguously specified and we are free to specify a constant somewhere in the problem. It is convenient to choose $P_- = 1$ so (2.9) a, b may now be written

$$p' = [\beta e^{iKz} + e^{-iKz}]\, e^{-i(\omega t + \overline{M}_i Kz)}$$
$$u' = [\beta e^{iKz} - e^{-iKz}]\, e^{-i(\omega t + \overline{M}_i Kz)} \qquad (2.13)a, b$$

For later computations, it is helpful to express these formulas in terms of their magnitudes and phases. First write the quantity β as

$$|\beta| = \left[\frac{(1+A_{or})^2 + A_{oi}^2}{(1-A_{or})^2 - A_{oi}^2}\right]^{\frac{1}{2}}$$

$$\beta = |\beta| e^{i\varphi} \qquad (2.14)a, b$$

$$\tan\varphi = \frac{-2A_{oi}}{1 - (A_{or}^2 + A_{oi}^2)}$$

Then the pressure and velocity fields can eventually be put in the form

$$p' = P\, e^{-i(\omega t + \overline{M}_i Kz - \psi_p)}$$
$$u' = \frac{1}{\overline{\rho}_i \overline{a}_i} U\, e^{-i(\omega t + \overline{M}_i Kz - \psi_u)} \qquad (2.15)a, b$$

where

$$P = 1 + |\beta|^2 + 2|\beta| \cos(2Kz + \varphi) \qquad (2.16)$$

$$U = 1 + |\beta|^2 - 2|\beta| \cos\varphi \qquad (2.17)$$

$$\tan\psi_p = \frac{-\sin Kz + |\beta| \sin(Kz+\varphi)}{\cos Kz + |\beta| \cos(Kz+\varphi)} \qquad (2.18)$$

$$\tan\psi_u = \frac{\sin Kz + |\beta| \sin(Kz+\varphi)}{-\cos Kz + |\beta| \cos(Kz+\varphi)} \qquad (2.19)$$

It is particularly important to note that the distributions of amplitudes and phases depend only on the Mach number of the flow and on the admittance function for the upstream boundary. In Section IV this feature is examined further with some data.

2.3 Acoustic Field in the Combustion Chamber

The mode shapes observed in the combustion chamber appear to be very different in LFRED and LIFRAM. Figure 3 shows the approximate shapes; data are given in Section IV. The sketches are incomplete and do not clearly show phase relationships. The oppositely directed arrows in Figure 3 (a) are intended to emphasize that there is approximately a π phase difference between the pressure oscillations in the two ends of the chamber in LFRED. In

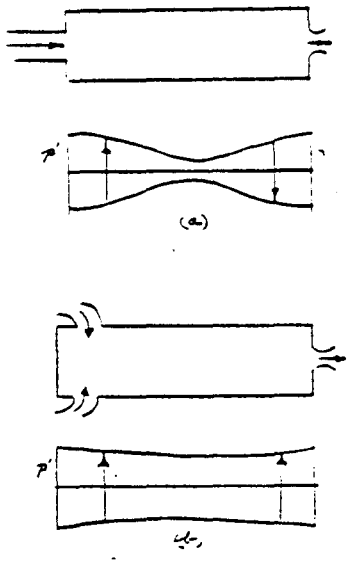

Fig. 3. Sketches of the Mode Shapes Observed in the Combustion Chambers.

contrast, the pressure field sketched in Figure 3 (b) for LIFRAM appears to be in phase throughout the chamber. Only the envelopes are shown in Figure 3; there is no node shown in 3 (a) because the position of pressure node actually fluctuates during a cycle of oscillation.

Those results suggest that the oscillation in LFRED consists primarily of the fundamental longitudinal mode, while that in LIFRAM is dominated by a bulk oscillation. But both apparently contain measurable proportions of other modes. This situation can be treated with the general analysis constructed first in reference 5 and later applied to bulk modes in reference 6. Briefly, the formal task is to determine the natural modes and frequencies for the problem defined by the inhomogeneous wave equation with inhomogeneous boundary condition:

$$\nabla^2 \hat{p} + k_c^2 \hat{p} = \hat{h} \qquad (2.20)$$

$$\hat{n} \cdot \nabla \hat{p} = -\hat{f} \qquad (2.21)$$

In general the functions $\hat{h}$ and $\hat{f}$ contain all influences of combustion, mean flow and the boundary conditions. The wavenumber k_c differs from k used above because the speed of sound is different in the combustion chamber: $k_c = (\overline{a}_c/\overline{a}_i)k$.

The solution to this problem is conveniently expressed in terms of Green's function chosen to satisfy the same wave operator and homogeneous boundary conditions:

$$\nabla^2 G + k_c^2 G = \delta(\vec{r} - \vec{r}_o) \qquad (2.22)$$

$$\hat{n} \cdot \nabla G = 0 \qquad (2.23)$$

Multiply (2.20) by G, (2.22) by $\hat{p}$, subtract

and integrate over the volume to find

$$\int [G\nabla^2 \hat{p} - \hat{p}\nabla^2 G]\, dV = \int G\hat{h}dV - \int \hat{p}\delta(\vec{r} - \vec{r}_o)dV$$

Substitute (2.21) and (2.23) and use Green's theorem:

$$\hat{p}(\vec{r}_o) = \int G(\vec{r}/\vec{r}_o)\,\hat{h}dV + \oiint G(\vec{r}/\vec{r}_o)\hat{f}\,dS$$

Finally, interchange $\vec{r}$ and $\vec{r}_o$, and use the property of G,

$$G(\vec{r}\,|\,\vec{r}_o) = G(\vec{r}_o\,|\,\vec{r})$$

to find

$$\hat{p}(\vec{r}) = \int G(\vec{r}\,|\,\vec{r}_o)\hat{h}_o\, dV_o + \oiint G(\vec{r}\,|\,\vec{r}_o)\hat{f}_o\, dS_o \quad (2.24)$$

This is the exact general solution but it is of no value without an explicit formula for G. The most useful form for use here is an expansion in the normal modes. Write

$$G = \sum A_N \psi N(\vec{r}) \quad (2.25)$$

where

$$\nabla^2 \psi_N + k_N^2 \psi_N = 0 \quad (2.26)$$

$$\hat{n} \cdot \nabla \psi_N = 0 \quad (2.27)$$

Substitute (2.25) into (2.22) and use (2.26) to find:

$$\sum (k^2 - k_N^2) A_N \psi_N = \delta(\vec{r} - \vec{r}_o) \quad (2.28)$$

Now multiply by ψ_M and integrate over volume. We assume that the ψ_N are orthogonal:

$$\int \psi_M \psi_N dV = E_M^2 \delta_{MN} \quad (2.29)$$

The coefficients are then found to be

$$A_M = \frac{\psi_M(\vec{r}_o)}{E_M^2(k_c^2 - k_M^2)} \quad (2.30)$$

Equation (2.25) for G is now explicit:

$$G = \sum \frac{\psi_N(\vec{r})\psi_N(\vec{r}_o)}{E_N^2(k_c^2 - k_N^2)} \quad (2.31)$$

Now use (2.31) in (2.24) to give the mode shape in the presence of the perturbations $\hat{h}$ and $\hat{f}$:

$$\hat{p}(\vec{r}) = \sum \frac{\psi_N(\vec{r})}{E_N^2(k_c^2 - k_N^2)} \left[\int \psi_n \hat{h}_c dV_o + \oiint \psi_N \hat{f}\, dS_o\right] \quad (2.32)$$

The unperturbed bulk mode is $\psi_o = 1$ with $k_o = 0$, so for the case of longitudinal oscillations only, in a chamber of length $L_c = L - L_i$,

$$\begin{aligned}
\psi_o &= 1 & k_o &= 0 \\
\psi_1 &= \cos(\pi \frac{z-L_i}{L_c}) & k_1 &= \frac{\pi}{L_c} \\
\psi_2 &= \cos(2\pi \frac{z-L_i}{L_c}) & k_2 &= \frac{2\pi}{L_c} \quad (2.33)^* \\
\psi_3 &= \cos(3\pi \frac{z-L_i}{L_c}) & k_3 &= \frac{3\pi}{L_c} \\
&\vdots & &\vdots
\end{aligned}$$

For both LFRED and LIFRAM we are concerned with oscillations which appear to be dominated by a single mode--the bulk mode, ψ_o in LIFRAM and the first wave mode ψ_1, in LFRED. For these cases $\hat{p} \sim \psi_o$ plus distortions and $\hat{p} \sim \psi_1$ plus distortions. In order to extract these forms from (2.32), the coefficients of ψ_o and ψ_1 respectively must be unity, giving the results for the actual mode shapes and wave numbers:

LIFRAM

$$\hat{p} = \psi_o + \sum^{N\geq 1} \frac{\psi_N(\vec{r})}{E_N^2(k_c^2 - k_N^2)} \times \left\{\int \psi_N \hat{h}_o dV_o + \oiint \psi_N \hat{f}_o\, dS_o\right\} \quad (2.34)$$

$$k^2 = \frac{1}{E_o^2}\left\{\int \hat{h}_o dV_o + \oiint \hat{f}_o dV_o\right\} \quad (2.35)$$

LFRED

$$\hat{p} = \psi_1 + \sum^{N\neq 1} \frac{\psi_N(\vec{r})}{E_N^2(k_c^2 - k_N^2)} \times \left\{\int \psi_N \hat{h}_o dV_o + \oiint \psi_N \hat{f}_o\, dS_o\right\} \quad (2.36)$$

$$k^2 = k_1^2 + \frac{1}{E_1^2}\left\{\int \psi_1 \hat{h}_o dV_o + \oiint \psi_1 \hat{f}_o\, dS_o\right\} \quad (2.37)$$

If only the bulk and first wave modes are significant, then the mode shapes are simpler:

*The origin z = 0 is always at the shock, so $z - L_i = 0$ at the entrance to the combustion chamber.

LIFRAM $$p' = 1 + \cos(\pi \frac{z-L_i}{L_c}) \times \frac{\int \psi_1 \hat{h}_c dV_o + \oiint \psi_1 \hat{f}_o dS_o}{E_1^2(k_c^2 - k_1^2)} \quad (2.38)$$

LFRED $$p' = \cos(\pi \frac{z-L_i}{L_c}) + \frac{\int \hat{h}_o dV_o + \oiint \hat{f}_o dS_o}{E_o^2 k_c^2} \quad (2.39)$$

We shall use only the results to first order, so in (2.38), $k_c^2 \approx 0$ and in (2.36), $k_c^2 \approx k_1^2 = \frac{\pi^2}{L_c^2}$; also, $E_o^2 = V$ and $E_1^2 = V/2$ where V is the volume of the chamber, so the formulas for the mode shapes are:*

LIFRAM $$\hat{p}(\vec{r}) = 1 - \frac{2L_c^2}{\pi^2 V} \cos(\pi \frac{z-L_i}{L_c}) \times \{\int \cos(\pi \frac{z-L_i}{L_c}) \hat{h} dV_o + \oiint \cos(\pi \frac{z-L_i}{L_c}) \hat{f} dS_o\} \quad (2.40)$$

LFRED $$\hat{p}(\vec{r}) = \cos(\pi \frac{z-L_i}{L_c}) + \frac{L_c^2}{\pi^2 V} \times \{\int \hat{h}_o dV_o + \oiint \hat{f}_o dS_o\} \quad (2.41)$$

In general, $\hat{h}$ and $\hat{f}$ are complex quantities, making the mode shapes complex functions of position. This can be interpreted as a phase shift in time, depending on position in the chamber as shown already by (2.15). To illustrate further, write the time-varying pressure fluctuation as

$$p'(\vec{r}, t) = \hat{p}(\vec{r}) e^{-i\omega t} = (\hat{p}^{(r)} + i\hat{p}^{(i)}) e^{-i\omega t} = |\hat{p}| e^{i(-\omega t + \varphi)} \quad (2.42)$$

where

$$|\hat{p}| = [(\hat{p}^{(r)})^2 + (\hat{p}^{(i)})^2]^{\frac{1}{2}} \quad (2.43)$$

$$\tan \varphi = \frac{\hat{p}^{(i)}}{\hat{p}^{(r)}} \quad (2.44)$$

*Note that the fields are normalized by taking the first term in (2.40), and the coefficient of the first term in (2.41) both to be unity.

Obviously, if $\hat{p}^{(i)} = 0$ then $\varphi = 0$, or $\varphi = \pi$, the classical case for no losses. But for $\hat{p}^{(i)} \neq 0$ there is a phase shift $\tan^{-1}(\hat{p}^{(i)}/\hat{p}^{(r)})$ which varies with position. Moreover, in general $|\hat{p}|$ will not exhibit a node because $\hat{p}^{(i)}$ and $\hat{p}^{(r)}$ will not simultaneously vanish. Thus, the envelope of the oscillations, as sketched in Figure 3(a), does not show a zero.

2.4 Joining the Solutions for the Inlet and Combustion Chamber

The formulas (2.40) and (2.41) for the pressure field in the combustion chamber must be coupled to the field in the inlet. That procedure will eventually produce a formula determining the frequency of oscillations in the entire device. The coupling occurs at the interface of the inlet and combustor and is expressed formally by requiring that the acoustic pressure and mass flux be continuous. Figure 4 shows the relevant items. Subscript $(\ )_{1\pm}$ denotes values

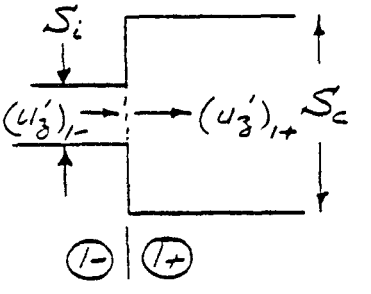

Fig. 4. Sketch Showing Matching at the Inlet/Combustor Interface.

at the interface; the conditions to be satisfied are

$$p'_{1-} = p'_{1+} \quad (2.45)$$

$$(u'_z S)_{1-} = (u'_z S)_{1+} \quad (2.46)$$

Note that the discontinuity in area must be accounted for as shown by (2.46). Now on the upstream side, according to remarks in Section 1.1, $(u'_z)_{1-} = \vec{u}' \cdot \hat{n}$ and on the downstream side, $(u'_z)_{1+} = -\vec{u}'_c \cdot \hat{n}$ where u'_c is the acoustic velocity in the combustion chamber. Thus we may write the combination of (2.45) and (2.46) in the form of an admittance function to be applied as a boundary condition on the waves in the combustion chamber. First divide (2.46) by (2.45).

$$\frac{(u'_z S)_{1-}}{p'_{1-}} = \frac{(u'_z S)_{1+}}{p'_{1+}}$$

Assume that the speeds of sound and average pressures are different in the two regions, so the normalized form of the last relation is

$$\frac{u'_{zi}/\bar{a}_i}{p'_i/\gamma\bar{p}_i}\left(\frac{\bar{a}_i}{\gamma\bar{p}_i}\right)S_i = \frac{-\vec{u}'_c\cdot\hat{n}/\bar{a}_c}{p'_c/\gamma\bar{p}_c}\left(\frac{\bar{a}_c}{\gamma\bar{p}_c}\right)S_c$$

$$= -A_{i+}\left(\frac{\bar{a}_c}{\gamma\bar{p}_c}\right)S_c \qquad (2.47)$$

where A_{i+} stands for the combination $(u'_c\cdot\hat{n}/p'_c)(\gamma\bar{p}_c/\bar{a}_c)$. Now u'_{zi} and p'_i are given by (2.15) a, b evaluated at $z = L_i$, so

$$\frac{u'_{zi}/\bar{a}_i}{p'_i/\gamma\bar{p}_i}\left(\frac{\bar{a}_i}{\gamma\bar{p}_i}\right) = \frac{1}{\bar{p}_i\bar{a}_i}\frac{U}{\bar{P}}e^{i(\psi_u-\psi_p)} \qquad (2.48)$$

Hence according to (2.47) the admittance A_{i+} presented to the combustion chamber by the inlet is

$$A_{i+} = -\left(\frac{\bar{p}_c\bar{a}_c}{\bar{p}_i\bar{a}_i}\right)\frac{S_i}{S_c}e^{i(\psi_u-\psi_p)} \qquad (2.49)$$

Because ψ_u, ψ_p are both real, the magnitude of A_{i+} is always the ratio of the characteristic acoustic impedances, multiplied by the area ratio, the result to be expected from classical acoustics.

The functions $\hat{h}$ and $\hat{f}$ are deduced from the general conservation equations. For the purposes here, eq. (7) in reference 6 applies, with the addition of a term representing the contribution from fluctuations of heat release. Thus, we have

$$\int\psi_N\hat{h}_o\,dV_o + \oint\!\!\oint\psi_N\hat{f}_o\,dS_o = i\bar{a}k_c\left[\oint\!\!\oint\psi_N^2\vec{\bar{M}}\cdot\hat{n}\,dS_o + \oint\!\!\oint\psi_N^2\,A\,dS_o - \frac{R}{\bar{a}_c\bar{p}_cC_v}\int\frac{Q'}{p'/\gamma\bar{p}_c}\psi_N^2\,dV_o\right]$$

Because of continuity of the mean flow, the first term vanishes; $\psi_N^2 = 1$ at both ends, so

$$\oint\!\!\oint\psi_N^2\vec{\bar{M}}\cdot d\vec{S}_o = -\bar{M}_iS_i + \bar{M}_nS_n = 0$$

The second term is

$$\oint\!\!\oint\psi_N^2A\,dS = A_{i+}S_i + A_nS_n$$

where A_n is the admittance of the exhaust nozzle. We have now

$$\int\psi_N\hat{h}_o\,dV_o + \oint\!\!\oint\psi_N\hat{f}_o\,dS_o = ik_c\left[A_{i+}S_i + A_nS_n - \frac{R}{\bar{a}_c\bar{p}_cC_v}\int\frac{Q'}{p'/\gamma\bar{p}_c}\psi_N^2\,dV_o\right] \qquad (2.50)$$

where (2.49) is to be used for A_{i+}. This result is required for the right hand sides of (2.35), (2.37), (2.40) and (2.41). The two cases, LFRED and LIFRAM will now be treated separately.

2.4.1 Acoustic Field in LFRED

The proposal is that the acoustic field is dominated by the fundamental wave modes in both the inlet and combustion chambers. Distortion in the inlet is caused by interaction with the inlet shock system and with the waves in the combustion chamber. Variations of cross-section area also influence the wave system but probably to a lesser extent. In any case, the field in the inlet is assumed to be well approximated by the fundamental mode, slightly distorted according to eq. (2.15).

On the contrary, the data strongly suggest that in the combustion chamber the acoustic field suffers a strong distortion which involves a qualitative change of shape. It appears that while the wave mode is dominant, there is an important contribution from the bulk mode. That is the reason for including the second term in (2.41). Note that this form cannot be constructed by using a simple wave with complex amplitude and phase. To see this, expand such a function,

$$\cos\left(\frac{\pi(z-L_i)}{L_c}+\varphi_c\right) = \left[\cos\frac{\pi z}{L_i}\cos\left(\varphi_c-\frac{\pi L_i}{L_c}\right) - \sin\frac{\pi z}{L_i}\sin\left(\varphi_c-\frac{\pi L_i}{L_c}\right)\right]$$

The average value of this function is zero, while the second term of (2.41) represents a non-zero average value, a pressure fluctuation which has uniform phase in the chamber.

Note also that, unlike the treatment of the field in the inlet, the influence of the boundary conditions on the field in the chamber is not explicitly accounted for in (2.41). The field is assumed to be only slightly distorted in the vicinity of the inlet and exit planes, partly because the areas S_i and S_n are significantly smaller than the cross-section area S_c.

The two solutions to be joined are

Inlet* $\hat{p}_i = P\,e^{-i(\bar{M}_iKz - \psi_p)}$ (2.51)

*This is (2.15) a with the time dependence dropped.

Combustion Chamber

$$\hat{p}_c = \cos \pi\left(\frac{z-L_i}{L_c}\right) + \frac{ik_c L_c^2}{\pi^2 V}\left[A_{i+}S_i + A_n S_N - \frac{R}{\bar{a}_c \bar{p}_c C_v}\int \frac{Q'}{p'/\gamma \bar{p}_c} \cos\left(\frac{z_o - L_i}{L_c}\right) dV_o\right] \quad (2.52)$$

Equation (2.52) is (2.41) with (2.50) substituted for the brackets. Joining the two pieces (2.51) and (2.52) is achieved by satisfying the two conditions (2.48) and (2.49) that the acoustic pressure and mass flux be continuous. Use the formula (2.49) for the admittance A_{i+} assures continuity of the mass flux; continuity of the pressure required that (2.51) and (2.52) be equal at $z = L_i$, a condition which will fix the amplitude P of the wave in the

$$P = e^{i(\bar{M}_i L_i - \psi_p)}\left[1 + \frac{ik_c L^2}{\pi^2 V}\left[A_{i+}S_i + A_n S_n - S_c(q_{1r} + iq_{1i})\right]\right] \quad (2.53)$$

where

$$q_{1r} + iq_{1i} = \frac{R/C_v}{\bar{a}_c \bar{p}_c S_c}\int\left[\frac{Q'}{p'/\gamma \bar{p}_c} \times \cos \pi\left(\frac{z_o - L_i}{L_c}\right)\right] dV_o \quad (2.54)$$

Equations (2.51) and (2.52) are now explicit formulas for the mode shape. The only remaining task is to determine the complex wavenumber k. From eq. (2.37) with (2.50),

$$k_c^2 = \left(\frac{\pi}{L_c}\right)^2 + i\frac{2k_c}{V}\left[A_{i+}S_i + A_n S_n - S_c(q_{1r} + iq_{1i})\right] \quad (2.55)$$

Now insert (2.49) for A_{i+} to find

$$k_c^2 = \left(\frac{\pi}{L_c}\right)^2 + i\frac{2k_c}{L_c}\left[A_n\left(\frac{S_n}{S_c}\right) - \left(\frac{\bar{\rho}_i \bar{a}_i}{\bar{\rho}_c \bar{a}_c}\right)\left(\frac{S_i}{S_c}\right)^2 e^{i(\psi_n - \psi_p)} - (q_{1r} + iq_{1i})\right] \quad (2.56)$$

If the distribution of fluctuations of heat release is given, so q_{1r}, q_{1i} are known, this is a transcendental equation for the complex wavenumber.

2.4.2 Acoustic Field in LIFRAM

According to earlier remarks, and shown by (2.40), the acoustic field in the combustion chamber of LIFRAM seems to be dominated by the bulk mode. The arithmetic required to determine the mode shape and wavenumber is identical to the steps followed above. In the combustion chamber the pressure field is now approximated by the combination of (2.40) and (2.50):

$$\hat{p}_c = 1 - i\frac{2k_c L^2}{\pi^2 V}\cos \pi\left(\frac{z-L_i}{L_c}\right)\left[A_{i+}S_i + A_n S_n - \frac{R}{\bar{a}_c \bar{p}_c C_v}\int \frac{Q'}{p'/\gamma \bar{p}_c} dV_o\right] \quad (2.57)$$

The field in the inlet is always given by (2.51), which, when equated to (2.57) at $z = L_i$ gives P for this case:

$$P = e^{i(\bar{M}_i L_i - \psi_p)}\left[1 - i\frac{2k_c L^2}{\pi^2 V}\left[A_{i+}S_i + A_n S_n - S_c(q_{0r} + iq_{0i})\right]\right] \quad (2.58)$$

with

$$q_{or} + iq_{0i} = \frac{R/C_v}{\bar{a}_c \bar{p}_c S_c}\int \frac{Q'}{p'/\gamma \bar{p}_c} dV_o \quad (2.59)$$

Substitution of (2.50), with $\psi_n = \cos \pi(z-L_i)/L_c$ into (2.35) provides

$$k_c = i\frac{1}{V}\left[A_{i+}S_i + A_n S_n - S_c(q_{0r} + iq_{0i})\right] \quad (2.60)$$

Finally, with (2.49) for A_{i+} we have the formula for the complex wavenumber:

$$k_c = \frac{i}{L_c}\left[A_n\frac{S_n}{S_c} - \left(\frac{\bar{\rho}_i \bar{a}_i}{\bar{\rho}_c \bar{a}_c}\right)\left(\frac{S_i}{S_c}\right)^2 e^{i(\psi_u - \psi_p)} - (q_{0r} + iq_{0i})\right] \quad (2.61)$$

Once again, like (2.56), this is an equation for the complex wavenumber, but the distribution of fluctuations of heat release must be known to obtain numerical values.

III. Admittance Function for a Normal Shock

Consider a normal shock initially stationary in a diverging duct, as sketched in Figure 5. Conditions upstream of the shock are supposed to be constant in time, although non-uniform in space. The problem is to determine the response of the shock to a sinusoidal fluctuation of pressure, p_4, immediately downstream of the shock. This motion produces a velocity fluctuation, u_4; the admittance function for the shock, denoted A_o above, is proportional to u_4/p_4.

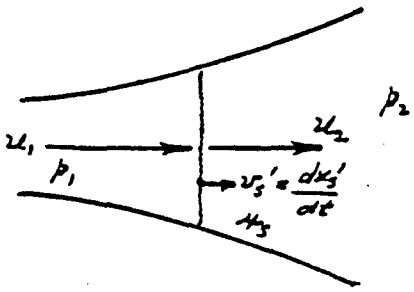

Fig. 5. Sketch of a Normal Shock in a Diverging Channel.

3.1 Quasi-Steady Behavior of a Shock Wave

We assume that the frequency of the fluctuation is sufficiently low that the shock responds in a quasi-steady fashion so that the problem can be solved by examining perturbations of the relations governing the behavior of a normal shock in steady flow

$$u_2 = u_1 \left[\frac{(\gamma-1)M_1^2 + 2}{(\gamma+1)M_1^2}\right] \tag{3.1}$$

$$p_2 = p_1 \left[\frac{2\gamma M_1^2 - (\gamma-1)}{\gamma+1}\right] \tag{3.2}$$

When the shock moves, the upstream conditions presented to the shock fluctuate for two reasons: because the shock has a velocity fluctuation itself, and because it moves through the non-uniform average flow field. Thus the fluctuation of upstream velocity, u_1', for the conventions defined in Figure 5, is

$$u_1' = -V_s' + \frac{du_1}{dx}\cdot x_s' \tag{3.3}$$

A fluctuation of the speed of sound is also presented to the shock,

$$a_1' = \frac{da_1}{dx}\cdot x_s' \tag{3.4}$$

and the associated fluctuation of the Mach number is

$$M_1' = -\frac{1}{a_1} V_s' + \frac{dM_1}{dx}\cdot x_s' \tag{3.5}$$

Finally, the shock experiences the fluctuation of upstream pressure due to its displacement,

$$p_1' = \frac{dp_1}{dx} x_s' \tag{3.6}$$

The derivatives of the mean flow properties in (3.3) - (3.6) are deduced from the shape of the duct, but the shock displacement, x_s', and velocity $V_s' = dx_s'/dt$ must be computed as part of the solution, with u_2'.

The assumption of quasi-steady behavior implies that the relations (3.1) and (3.2) for steady flow may be used with the variables replaced by the sums of steady values plus fluctuations; set $u_1 \rightarrow u_1 + u_1'$, etc., in (3.1) and (3.2), and eventually the formulas can be deduced.

$$u_2' = a_1 [V_x x_s' + V_v v_s'] \tag{3.7}$$

$$p_2' = p_1 [P_x x_s' + P_v v_s'] \tag{3.8}$$

where

$$V_x = -\frac{2}{(\gamma+1)M_1^2}\frac{dM_1}{dx} \tag{3.9}$$

$$V_v = \frac{\gamma-1}{a_1}\frac{(M_\beta^2 - M_1^2)}{(\gamma+1)M_1^2} \tag{3.10}$$

$$P_x = \frac{2\gamma M_1}{(\gamma+1)}\frac{(M_\alpha^2 - M_1^2)}{(1+\frac{\gamma-1}{2}M_1^2)}\frac{dM_1}{dx} \tag{3.11}$$

$$P_v = -\frac{1}{a_1}\frac{4\gamma M_1}{(\gamma+1)} \tag{3.12}$$

and

$$M_\alpha = \left(\frac{\gamma+3}{2}\right)^{\frac{1}{2}} \tag{3.13}$$

$$M_\beta = \left(\frac{2}{\gamma-1}\right)^{\frac{1}{2}} \tag{3.14}$$

The Mach numbers M_α and M_β are special. When $M_1 = M_\beta$, V_v vanishes and the velocity fluctuation (3.7) downstream of the shock depends only on the shock displacement and is proportional to the gradient of the average Mach number upstream of the shock. Thus in a uniform duct, $dM_1/dx = 0$, no velocity fluctuation is produced by the shock wave in response to a pressure fluctuation downstream and the wave appears as a rigid surface.

If $M_1 = M_\alpha$, $P_x = 0$, and a small displacement of ths shock produces no change in the pressure downstream. The significance of the Mach number M_α has been noted by Crocco (ref. 7). Interpretation of both M_α and M_β are more clearly understood by writing (3.7) and (3.8) in the forms of Taylor's series expansions to first order:

$$\delta u_2 = \left(\frac{\partial u_2}{\partial x_s}\right)_{v_s} \delta x_s + \left(\frac{\partial u_2}{\partial v_s}\right)_{x_s} \delta v_s \tag{3.15}$$

$$\delta p_2 = \left(\frac{\partial p_2}{\partial x_s}\right)_{v_s} \delta x_s + \left(\frac{\partial p_2}{\partial v_s}\right)_{x_s} \delta v_s \tag{3.16}$$

We consider only the two partial derivatives which vanish at the Mach number M_α or M_β. First note that

$$\left(\frac{\partial p_2}{\partial x_s}\right)_{v_s} = \left(\frac{dp_2}{dM_1}\right)_0 \left(\frac{dM_1}{dx_s}\right) \tag{3.17}$$

where $(\ )_0$ indicates that the derivative is to be taken with the upstream stagnation conditions

fixed. One may then easily show that

$$\left(\frac{dp_s}{dM_1}\right)_o = p_1 \frac{2\gamma M_1}{\gamma+1} \frac{(M_\alpha^2 - M_1^2)}{(1+\frac{\gamma-1}{2} M_1^2)} \qquad (3.18)$$

Thus (3.17) is exactly $p_1 P_x$ as required in (3.8), and M_α is indeed the value of upstream Mach number at which the downstream static pressure reaches a stationary value (it is in fact a maximum) as the upstream Mach number is changed with the upstream stagnation pressure fixed.

To compute $(\partial u_s / \partial v_s)_{x_s}$ let $u_1 \to u_1 - v_s$ in (3.1):

$$u_s = (u_1 - v_s) \left[\frac{(\gamma-1)\frac{(u_1-v_s)^2}{a_1^2} + 2}{(\gamma+1)\frac{(u_1-v_s)^2}{a_1^2}} \right]$$

It is easy to show that if the ambient speed of sound is held constant, this expression leads to

$$\left(\frac{\partial u_s}{\partial v_s}\right)_{a_1} = (\gamma-1) \frac{(M_\beta^2 - M_1^2)}{(\gamma+1) M_1^2} \qquad (3.19)$$

which is $a_1 V_v$ in (3.7). Note that this result implies that requiring the shock position to be fixed, as specified initially, is equivalent to fixing the upstream static conditions. The reason is that formally the shock is fixed in position relative to the observer by superposing the suitable uniform speed on the entire field. Thus the fluid upstream suffers a change of speed $(-v_s)$ which means that for the observer stationary relative to the shock, the stagnation conditions are changed but the static conditions are not, when compared with the case when the shock is observed to move.

For comparison with calculations reported in reference 8, we use (3.7) and (3.8) to form an expression for the shock displacement when a steady oscillation is imposed on the downstream pressure. Then $v_s' = -i\omega x_s' = -i\omega \hat{x}_s' \exp(-i\omega t)$. With the exponential time factors dropped, (3.7) and (3.8) become

$$\hat{u}_s = a_1 [V_x - i\omega V_v] \hat{x}_s \qquad (3.13)$$

$$\hat{p}_s = p_1 [P_x - i\omega P_v] \hat{x}_s \qquad (3.14)$$

Let $\hat{x}_{s_o}$ denote the amplitude of the displacement when $\omega = 0$; then the last two equations give

$$\frac{\hat{x}_s}{\hat{x}_{s_o}} = \frac{1}{1 - i\omega \frac{V_v}{V_x}} \quad (\hat{u}_s \text{ forcing}) \qquad (3.15)$$

$$\frac{\hat{x}_s}{\hat{x}_{s_o}} = \frac{1}{1 - i\omega \frac{P_v}{P_x}} \quad (\hat{p}_s \text{ forcing}) \qquad (3.16)$$

These are the expressions for the frequency response of the shock wave, differing of course for the two cases corresponding to oscillations of downstream pressure or velocity.

Figures 6 and 7 show the magnitude and phase of the shock displacement normalized with

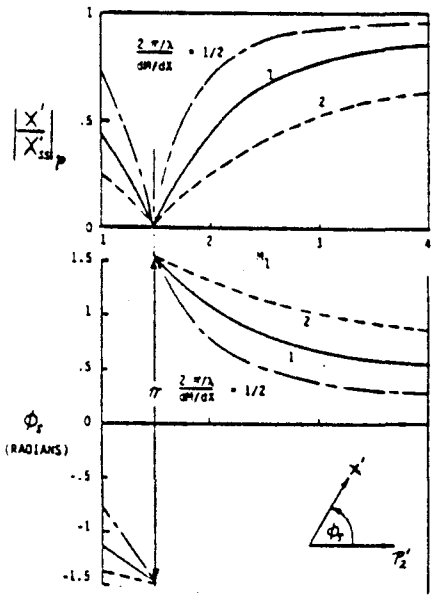

Fig. 6. Normal Shock Displacement: Response to a Downstream Pressure Fluctuation.

respect to the values for $\omega = 0$, given by (3.15) and (3.16). Note that there is considerable dependence on both the Mach number upstream of the shock as well as its gradient. This is a significant difference from the result first reported in reference 9 and subsequently widely used.

The reason for the difference arises from differences in the manner of handling conditions downstream of the shock wave. In reference 9, the forcing disturbance is supposed to exist at some plane displaced from the shock wave. Some additional computations are required to connect that disturbance with the fluctuations immediately downstream of the shock wave. Here we suppose, on the contrary, that the forcing disturbance (e.g. an acoustic wave) extends to the downstream edge of the shock. We therefore do not require the additional computations noted, which we believe should not be included whenever effects of the shock wave are to be accounted for as part of a boundary condition.

More useful for the analysis constructed in Section II is the admittance function,

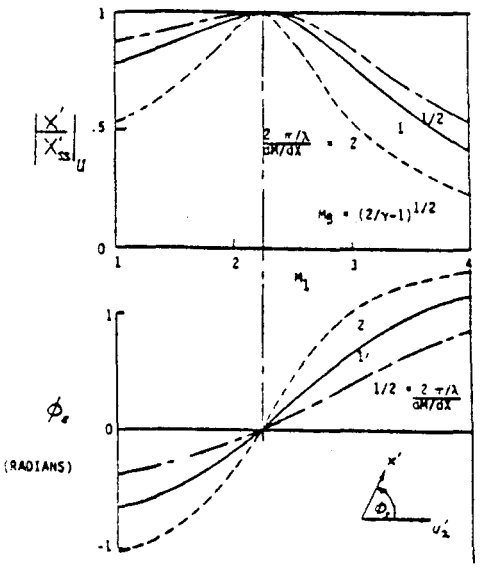

Fig. 7. Normal Shock Displacement: Response to a Downstream Velocity Fluctuation.

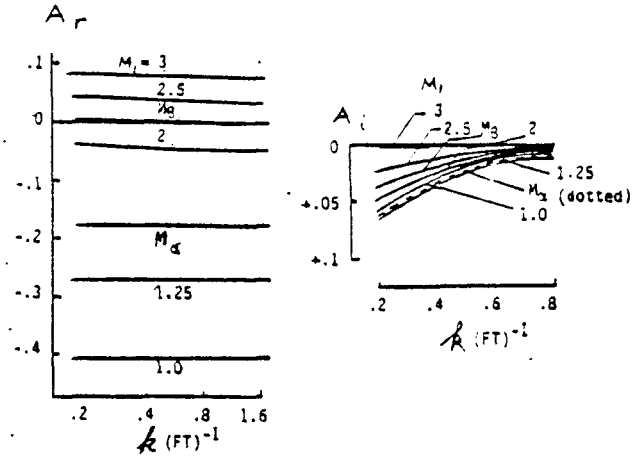

Fig. 8. Admittance Function for a Normal Shock: dM/dx = 0.04 ft.$^{-1}$.

proportional to the ratio of (3.13) and (3.14). Note that the properties downstream of the shock are those appropriate to the inlet, so $M_e = \overline{M}_i$ etc. Substitution into (2.11) gives

$$A_o = \frac{1}{\gamma} \frac{\overline{\rho}_i \overline{a}_i}{\rho_1 a_1} \frac{V_x - i\omega V_v}{P_x - i\omega P_v} \qquad (3.17)$$

This is strongly dependent on three quantities: the frequency, the Mach number upstream of the shock wave and the gradient of the Mach number at the location of the shock wave. The real and imaginary parts of (3.17) are

$$A_{or} = \frac{1}{\gamma} \frac{\overline{\rho}_i \overline{a}_i}{\rho_1 a_1} \frac{V_x P_x - \omega^2 V_v P_v}{P_x^2 + \omega^2 P_v^2} \qquad (3.18)$$

$$A_{oi} = \frac{1}{\gamma} \frac{\overline{\rho}_i \overline{a}_i}{\rho_1 a_1} \frac{\omega(V_x P_v - V_v P_x)}{P_x^2 + \omega^2 P_v^2} \qquad (3.19)$$

Figures 8 through 10 show the real and imaginary parts of the admittance function for three values of the gradient of the Mach number, chosen to be useful in later discussion of the data. The dependence on the Mach number gradient is particularly striking.

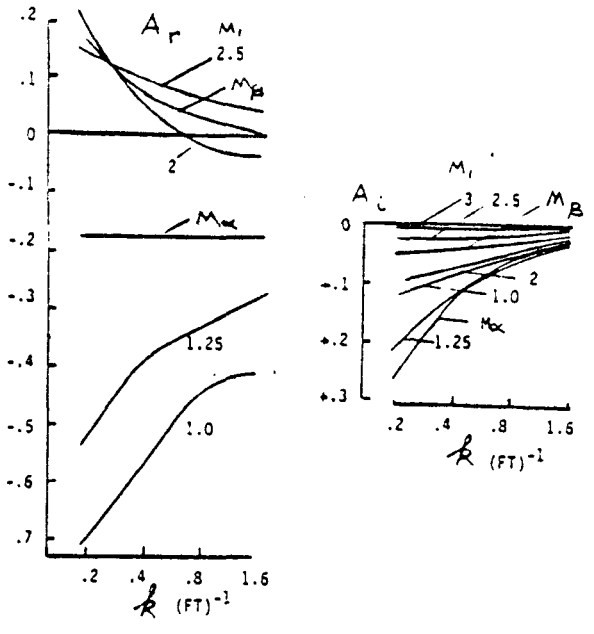

Fig. 9. Admittance Function for a Normal Shock: dM/dx = 0.4 ft.$^{-1}$.

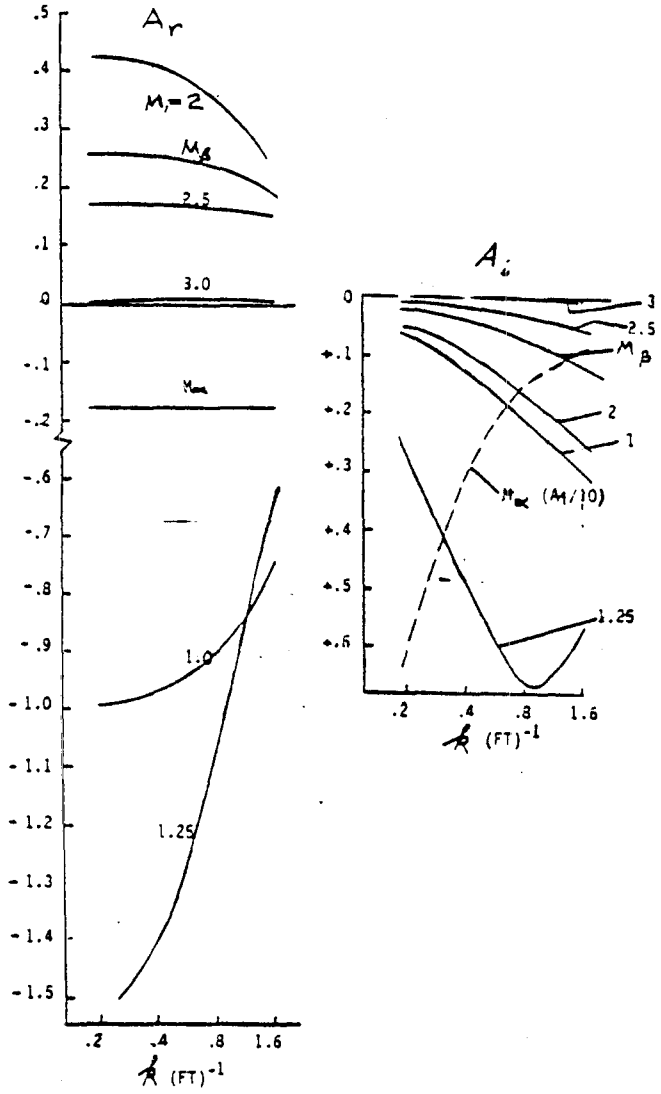

Fig. 10. Admittance Function for a Normal Shock: $dM/dx = 4.0$ ft.$^{-1}$.

IV. Distributions of Phase and Amplitudes

Figures 11 and 12 show the phase and amplitude distributions observed in the LFRED and LIFRAM engines. We now make use of the analyses constructed above to interpret qualitatively some of the features. The discussion is necessarily incomplete because at this time we have no detailed representation of the combustion processes.

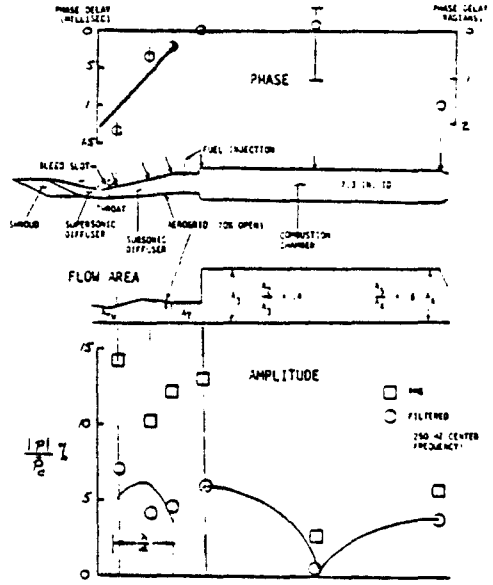

Fig. 11. Distributions of Phase and Amplitude Observed in LFRED.

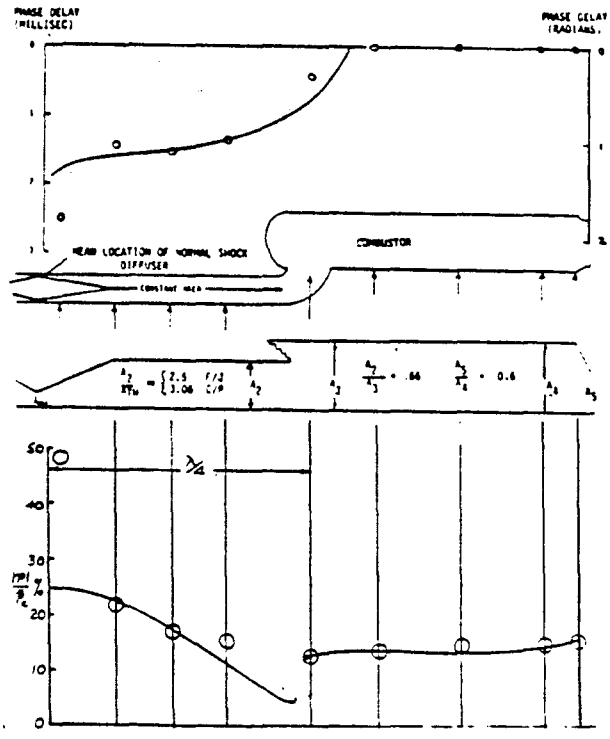

Fig. 12. Distributions of Phase and Amplitude Observed in LIFRAM.

	LFRED	LIFRAM
FREQUENCY HZ.	250	116
INLET		
$\bar{a}_i$ ft/sec	1610	1495
L_i ft	1.8	3.3 ($\approx \lambda/4$)
$\bar{M}_i$	.55	.25
λ ft	4.5	12.1
$(\lambda)_{\bar{M}=0}$ ft	6.4	12.9
$(\frac{dM}{dx})_{Shock}$ ft^{-1}	4	0.4
COMBUSTOR		
$\bar{a}_c$ ft/sec	2600	2600
L_c ft	4.8 ($\approx \lambda/2$)	3.9
λ ft	10.4	22.4

Table 1. Some Characteristics of the LFRED and LIFRAM Engines.

Table 1 is a compilation of the physical characteristics which will be used. The acoustic wavelengths have been calculated with estimated average speeds of sound and the observed frequencies. If the mean flow is ignored, $\lambda = a/f$, but if the mean flow Mach number is not small, then eq. (2.10) gives the value $\lambda = (1-M^2)(a/f)$; both values are given for the inlets.

The lengths given in Table 1 are approximate values, since the ends of the inlets and combustors are not precisely defined. Two conclusions are noted in the table: a quarter wave fits very closely in the inlet of LIFRAM; and a half wave nearly matches the combustion chamber of LFRED. These observations initiated the general approach taken here and described above in Sections I and II.

On the contrary, the inlet of LFRED spans only $2\frac{1}{2}$ wavelengths and the combustion chamber of LIFRAM seems to be nearly six wavelengths long. The first apparent discrepancy is due to distortion of the acoustic field by the large flow speed: note that in fact the length of the inlet is very closely one quarter of the wavelength calculated for zero flow speed. That a half wave is so much shorter than the combustion chamber of LIFRAM (i.e. the frequency of the waves is relatively lower than one would expect based on the behavior observed for LFRED appears at least partly to be due to the use of side dumps and partly to the fact that the inlet and combustion chamber have approximately the same length. Full resolution of this clear distinction between LFRED and LIFRAM must await subsequent work.

Thus it seems possible to explain qualitatively some of the structure shown by the data presented in Figures 11 and 12. The acoustic amplitude observed in the combustion chamber of LFRED seems dominated by a half-wave (the pressure fluctuation is largest at the ends and nearly vanishes at the center); and the amplitude in the inlet of LIFRAM is maximum at the forward end, and minimum at the aft end, so the field is approximately a quarter-wave.

Now consider in more detail the pressure field in the inlet, given by (2.15) a:

$$p' = Pe^{-i(\omega t + \bar{M}_i Kz - \psi_p)} \qquad (4.1)$$

$$P = 1 + |\beta|^2 + 2|\beta|\cos(2Kz + \varpi) \qquad (4.2)$$

$$\tan\psi_p = \frac{-\sin Kz + |\beta|\sin(Kz+\varpi)}{\cos Kz + |\beta|\cos(Kz+\varpi)} \qquad (4.3)$$

where, from eqs. (2.18) a, b:

$$|\beta| = \frac{(1+A_{or}^2) + A_{oi}^2}{(1-A_{or})^2 + A_{oi}^2} \qquad (4.4)$$

$$\tan\varpi = \frac{2A_{oi}}{(1-A_{or}^2) - A_{oi}^2} \qquad (4.5)$$

The distributions of amplitude and phase depend on frequency, Mach number, and the real and imaginary parts of the admittance function for the shock wave. For given frequency and Mach number-known from test results--the variations of amplitude and phase observed in the inlet should therefore provide quite specific information about the real and imaginary parts of the admittance function for the shock wave in the inlet. The inlet may be viewed essentially as an impedence tube which can be used to measure the impedance (or admittance) of the shock system in the diffuser section.

In Figures 11 and 12, the phase and amplitude distributions have been plotted with the values of frequency and Mach number listed in Table 1. The values for the real and imaginary parts of the admittance function used are indicated in the figures, and also in Figures 9 and 10 corresponding to LIFRAM and LFRED respectively. They are summarized in Table 2.

	LFRED	LIFRAM
$k = 2\pi/\lambda$ ft^{-1}	1	.5
M_1	1.2	1.6
$\frac{dM_1}{dx}$ ft^{-1}	4	0.4
A_{or}	-.9	-.15
A_{oi}	+1.0	+.15

Table 2. Summary of Values Used to Calculate the Amplitude and Phase Distributions Shown in Figures 11 and 12.

The agreement between the theory and the observations seems to be fairly good, if the approximations and uncertainties are recognized. Note that the predicted amplitudes for both LFRED and LIFRAM are unsatisfactory near the inlet/combustor junction. This is at last partly because we have ignored blockage by grids and injection hardware, and partly, especially for LIFRAM, because the one-dimensional approximation is not particularly good in the region. The large differences between the data points and the calculated values near the shock are partly due to uncertainties in the data: the pressure gage was very close to the shock and possibly the shock traversed the gage.

Perhaps more significantly, these results apparently verify that larger values of the gradient of Mach number at the shock location produce wider ranges of the real part of the admittance function; those can be either positive or negative depending on the upstream Mach number for the shock wave. This is a particularly important result of the analysis, for if the real part of the admittance is negative, according to the conventions followed here, the shock wave acts to attenuate acoustic waves.

To verify the last conclusion it is simplest to return to the formulation described in Section 2.1. According to eqs. 2.6, the amplitude P_4 of a small amplitude wave reflected from the shock is β times the amplitude P of the incident wave. The magnitude of β, given by eq. (2.14), is smaller than unity if $A_{or} < 0$. Thus a wave reflected from the shock wave suffers a reduction of amplitude: the shock will, under these conditions, extract energy from any acoustic waves sustained in the downstream region. It is a curious result that there are rather broad conditions (see Figures 8-10) when the shock wave will in fact add energy to the acoustic waves and is therefore a destabilizing influence.

The upstream Mach numbers for the inlet shocks are nearly the same for LFRED and LIFRAM. But the local gradient of Mach number is nearly ten times greater in LFRED, which produces a negative value of the real part of the admittance function more than three times larger than for LIFRAM. Thus, the shock should be, according to theory, substantially more effective in attenuating acoustic waves than is the case for LIFRAM. It may not be coincidental that in fact the amplitudes of oscillation observed in LFRED are generally much less than those exhibited by LIFRAM; compare Figures 11 and 12.

Now consider the pressure distributions in the combustion chamber, given by (2.52) and (2.57) with (2.49) substituted for A_{i_+}:

LFRED

$$\hat{p}_c = \cos\pi\frac{(z-L_i)}{L_c} + \frac{ik_cL_c}{\pi^2}\left[A_n\left(\frac{S_n}{S_c}\right) - \left(\frac{\bar{\rho}_i\bar{a}_i}{\bar{\rho}_c\bar{a}_c}\right)\left(\frac{S_i}{S_c}\right)^2 e^{i(\psi_u-\psi_p)} - (q_{1r}+iq_{1i})\right] \tag{4.6}$$

LIFRAM

$$\hat{p}_c = 1 - i\frac{2k_cL_c}{\pi^2}\cos\pi\frac{(z-L_i)}{L_c}\left[A_n\left(\frac{S_n}{S_c}\right) - \left(\frac{\bar{\rho}_i\bar{a}_i}{\bar{\rho}_c\bar{a}_c}\right)\left(\frac{S_i}{S_c}\right)^2 e^{i(\psi_u-\psi_p)} - (q_{0r}+iq_{0i})\right] \tag{4.7}$$

The wave number k_c in LFRED is given by (2.56), differing by a small amount from π/L_c; in the second term of (4.6) we may substitute $k_cL_c = \pi$. In (4.7) we use (2.61). The pressure distributions are therefore

LFRED

$$\hat{p}_c = \cos\pi\frac{(z-L_i)}{L_c} + i\left[A_n\frac{S_n}{S_c} - \left(\frac{\bar{\rho}_i\bar{a}_i}{\bar{\rho}_c\bar{a}_c}\right)\left(\frac{S_i}{S_c}\right)^2 e^{i(\psi_u-\psi_p)} - (q_{1r}+iq_{1i})\right] \tag{4.8}$$

LIFRAM

$$\hat{p}_c = 1 + \frac{2}{\pi^2}\cos\pi\frac{(z-L_i)}{L_c}\left[A_n\frac{S_n}{S_c} - \left(\frac{\bar{\rho}_i\bar{a}_i}{\bar{\rho}_c\bar{a}_c}\right)\left(\frac{S_i}{S_c}\right)^2 e^{i(\psi_u-\psi_p)} - (q_{0r}+iq_{0i})\right] \tag{4.9}$$

For the nozzle admittance function, A_n, it is sufficiently accurate to use the result $A_n = \bar{M}_n(\gamma+1)/2$ for a nozzle where length is short compared with the acoustic wavelength (ref. 10). Thus the only terms not known in (4.8) and (4.9) are those arising from the interactions with the combustion processes, q_0 and q_1, equations (2.54) and (2.59).

Define

$$\Delta_1 \equiv \Delta_{1r} + i\Delta_{1i} = A_n\frac{S_n}{S_c} - \frac{\bar{\rho}_i\bar{a}_i}{\bar{\rho}_c\bar{a}_c}\left(\frac{S_i}{S_c}\right)^2 \times e^{i(\psi_n-\psi_p)} - (q_{1r}+iq_{1i}) \tag{4.10}$$

$$\Delta_0 \equiv \Delta_{or} + i\Delta_{0i} = \frac{2}{\pi^2}\left[A_n\frac{S_n}{S_c} - \frac{\bar{\rho}_i\bar{a}_i}{\bar{\rho}_c\bar{a}_c}\left(\frac{S_i}{S_c}\right)^2 \times e^{i(\psi_u-\psi_p)} - (q_{1r}+iq_{1i})\right]^2 \tag{4.11}$$

and the pressure distributions may now be written in forms displaying explicity and the amplitudes and phases:

LFRED

$$\hat{p}_c = \left[\cos^2\pi\frac{(z-L_i)}{L_c} + |\Delta_1|^2\right]^{\frac{1}{2}} e^{i\varphi_{c_1}} \tag{4.12}$$

LIFRAM

$$\hat{p}_c = \left[1 + |\Delta_0|^2 \cos^2 \pi \frac{(z-L_i)}{L_c}\right]^{\frac{1}{2}} e^{i\varpi_{c_0}} \quad (4.13)$$

where

$$\tan\varpi_{c_1} = \frac{\Delta_{1r}}{\cos\pi \frac{(z-L_i)}{L_c} - \Delta_{1i}} \quad (4.14)$$

$$\tan\varpi_{c_0} = \frac{\Delta_{0i}}{1 + \Delta_{0r} \cos\pi \frac{(z-L_i)}{L_c}} \quad (4.15)$$

It is essential that the corrections represented by Δ_0 and Δ_1 be relatively small for these results to be valid. Thus according to (4.13) there should be in LIFRAM only small deviations from uniform amplitude and phase, a feature very obvious in the data shown in Figure 12.

Equation (4.12) shows that the amplitude distribution in the combustion chamber of LFRED should, as suggested in Figure 11, be very closely a half-wave. Note that the correction Δ_1^2, prevents the occurrence of a node ($\hat{p}_c = 0$). also shown by the data. The phase distribution is a bit more complicated. Suppose first that $\Delta_1 = 0$, so (4.14) is

$$\tan\varpi_{c_1} = \frac{0}{\cos\pi \frac{(z-L_i)}{L_c}}$$

If $z < L_i + L_c/2$, then $\varpi_{c_1} = \tan^{-1}(0/+|\cos Z|)$ while if $(L_i + L_c/2) < z < L_c$ then $\varpi = \tan^{-1}(0/-|\cos Z|)$ where $Z = \pi(z-L_i)/L_c$. But suppose $\Delta_1 \neq 0$ then for example at the aft end where $\cos\pi(z-L_i)/L_c = \cos\pi = -1$, $\tan\varpi_c = \Delta_{1r}/(-1 - \Delta_{1i}) \approx \Delta_{1r}/(-1)$ which gives $\pi < \varpi_c < \pi/2$ providing $\Delta_{1r} < 0$. This feature too appears in the data plotted in Figure 11: the phase difference between the fore and aft ends is only about 2 radians rather than π radians, the value for a classical half-wave.

The solid lines in Figures 11 and 12 are based on the preceding observations. Equations (4.2) and (4.3) give the amplitude and phase in the inlets; (4.12) and (4.13) give the amplitude and phase in the combustion chambers. Absolute values cannot be calculated. The analysis provides results for phase differences only, and because the theory is linear, the amplitude distribution contains an arbitrary multiplying constant whose value has been adjusted to provide reasonable fit to the data. At this time the values of the constants Δ_0 and Δ_1 are unknown so to this extent the predictions of the oscillations in the combustion chamber are necessarily qualitative. Demonstration that the apparently correct behavior predicted here really is that observed will require much more detailed analysis of the combustion processes. The analysis must eventually be combined with systematic tests specifically intended to provide accurate data for amplitude and phase distributions.

V. Concluding Remarks

The results described here must be regarded as only a beginning. We emphasize that the approach we advocate rests on an intimate joining of modeling, approximate analysis, and experimental results. The problems to be treated in ramjet engines are complicated and contain many uncertainties. It will not be productive to try to formulate elaborate theories treasured for their alleged predictive powers.

Solely because of the observed values of frequencies, there is little doubt that the oscillations we have treated involve predominantly fluctuating velocities parallel to the axis of the engine. Almost all geometrical complications have been ignored; the only deviation from an uniform duct is the abrupt change of area at the juction of the inlet and combustion chamber. The sort of analysis we have constructed here can be extended to accomodate considerably more general geometries. But even for the LIFRAM engine, the simple one-dimensional approximation seems to work quite well in many respects. A significant consequence is that it is quite easy to acquire appreciation for the dominant influences.

There is presently no reason to doubt that the sources of pressure oscillations in ramjet engines reside in the combustion chamber. That problem is accommodated by the analysis, but we have not treated it here. Therefore, even though the general analysis can be used to predict stability, we have not examined the conditions under which small disturbances are unstable. Thus, we make no predictions of oscillatory behavior in engines. Our purpose has been the more modest one of demonstrating as far as possible that an internally consistent description of observed oscillations can be constructed. An important aspect of this procedure is that we have examined both amplitude and phase. The importance of the relative phase is well-known, but its value in practical application has not often been recognized.

The very obvious differences between the structures of the acoustic modes within the combustion chambers of LFRED and LIFRAM seem to be due to differences in the inlet/combustion chamber-geometry. Ultimately, of course, the details of the combustion processes and flow must also be involved. It is a useful result of the analysis, that in both cases the acoustic field may be viewed as superpositions of a bulk mode, having uniform amplitude and phase within the chamber; and the fundamental wave mode for a closed chamber. The axial dump configuration favors excitation of the wave mode while the bulk mode is evidently more easily sustained, and therefore dominates, in the side dump configuration.

Longitudinal oscillations excited in the combustion necessarily leak upstream into the inlet. This is nearly a uniform duct, and one may view the combustion chamber as essentially a source of plane waves propagating upstream to the diffuser, there to be reflected back downstream to the exit of the inlet. Thus, the amplitude

attained by oscillations in the combustion chamber depends on the strength of the driving mechanism, associated with the combustion processes; on attenuation by the exhaust nozzle; and on the action of the inlet duct.

According to the model we have constructed here, the most important part of the inlet is the shock system in the diffuser which we represent as a single normal shock. Calculations of the admittance function--essentially the frequency response--for a normal shock wave exposed to small pressure oscillations downstream have led to two important conclusions. First, the admittance function is a strong function of three variables: the frequency of oscillations; the Mach number just upstream of the shock; and the gradient of Mach number at the location of the shock. Second, a normal shock wave may act either to attenuate or to amplify acoustic waves.

Comparisons of numerical results with observed values of amplitude and phase in the inlets of LFRED and LIFRAM shows that, for the data examined, the shock waves in both engines act to attenuate acoustic waves in the inlet. This conclusion follows from calculations which also demonstrate the predicted values of the admittance function for the shock wave are consistent with distributions of amplitude and phase observed in the inlets. The results are particularly interesting because the frequencies and values of Mach number gradient are very different in the two engines.

For practical purposes, the most significant general result of this work is that the shock system in the inlet exerts a strong, if not dominant, influence on oscillations excited in the combustion chamber. Specifically, the designer apparently has a direct control through choice of the Mach number gradient at the location of the shock wave in the diffuser. Of the two cases examined here, the more severe oscillations occurred in LIFRAM for which the gradient and, according to the analysis, attenuation by the shock wave, were lower. We emphasize that because of approximations central to the analysis, and because only limited data have been examined, these conclusions have not been firmly established beyond question. The matter clearly merits extensive study.

Acknowledgements

This work was sponsored in part by the Navy-Liquid Fuel Ramjet Engine Component Technology (N00123-77-C-0541) and by the Air Force-Liquid Fuel Ramjet Engine Demonstrator (F33615-76-C-2073) (LFRED) Programs.

References

1. Culick, F. E. C. "Report of the JANNAF Workshop on Pressure Oscillations in Ramjets", 1980 JANNAF Propulsion Meeting (March 1980); 17th JANNAF Combustion Meeting (September 1980).

2. Rogers, T. "Pressure Oscillations in Small Ramjet Engines", 16th JANNAF Combustion Meeting (September 1979) pp. 619-647.

3. Raushenbakh, B. V. Vibrational Combustion Translated from Russian, Foreign Technology Division, Wright Patterson Air Force Base, FTD TT 62-942.

4. Raushenbakh, B. V. et al, Physical Principles of the Working Process in Combustion Chambers of Jet Engines Ibid. FTD-MT-65-78.

5. Culick, F. E. C. "Acoustic Oscillations in Solid Propellant Rocket Motors", Astronautica Acta, V. 12, No. 2 (March-April 1966) pp. 113-126.

6. Culick, F. E. C. "Some Nonacoustic Instabilities in Rocket Chambers are Acoustic", AIAA J., V. 6, No. 7 (July 1968) pp. 1421-23.

7. Crocco, L. "One-Dimensional Treatment of Steady Gas Dynamics", in Fundamentals of Gas Dynamics, H. W. Emmons (Ed.) Princeton University Press, Princeton, NJ (1958).

8. Hurrell, H. G. "Analysis of Shock Motion in Ducts During Disturbances in Downstream Pressure", NACA TN 4090.

9. Crocco, L. and Cheng, S.-I. Theory of Combustion Instability in Liquid Propellant Rocket Motors. AGARDograph No. 8, Pergamon Press (1957) Appendix B.